

Supplemental Information for:

Challenges for Physical Characterization of Silver Nanoparticles Under Pristine and Environmentally Relevant Conditions

Robert I. MacCuspie, Kim Rogers, Manomita Patra, Zhiyong Suo, Andrew J. Allen, Matthew N. Martin, Vincent A. Hackley

Figure SI-1 below is designed to show that differences in image processing could inadvertently lead to incorrect conclusions. A rational approach to selecting a z-scale for image output may be to optimize the contrast of the nanoparticles of the nominal size, to see them most clearly, and to ensure that when sizing by cross-section analysis that the line includes points in the tallest region of the nanoparticle and thus measure the maximum nanoparticle height. However, this runs the risk of unintentionally removing very small nanoparticles from the image (one of the significant advantages of employing AFM), as highlighted by the placement of the black circles in the top and bottom rows, which could lead to their omission when preparing a histogram. This risk is greatest when the difference between the diameter of the small and large nanoparticle populations is greatest. Figure SI-2 shows a larger range of AgNP sizes and Z-scales to provide a visual feel for the nature of this effect. Briefly examining the image with conditions optimized to visualize very small AgNPs will ensure that this does not occur.

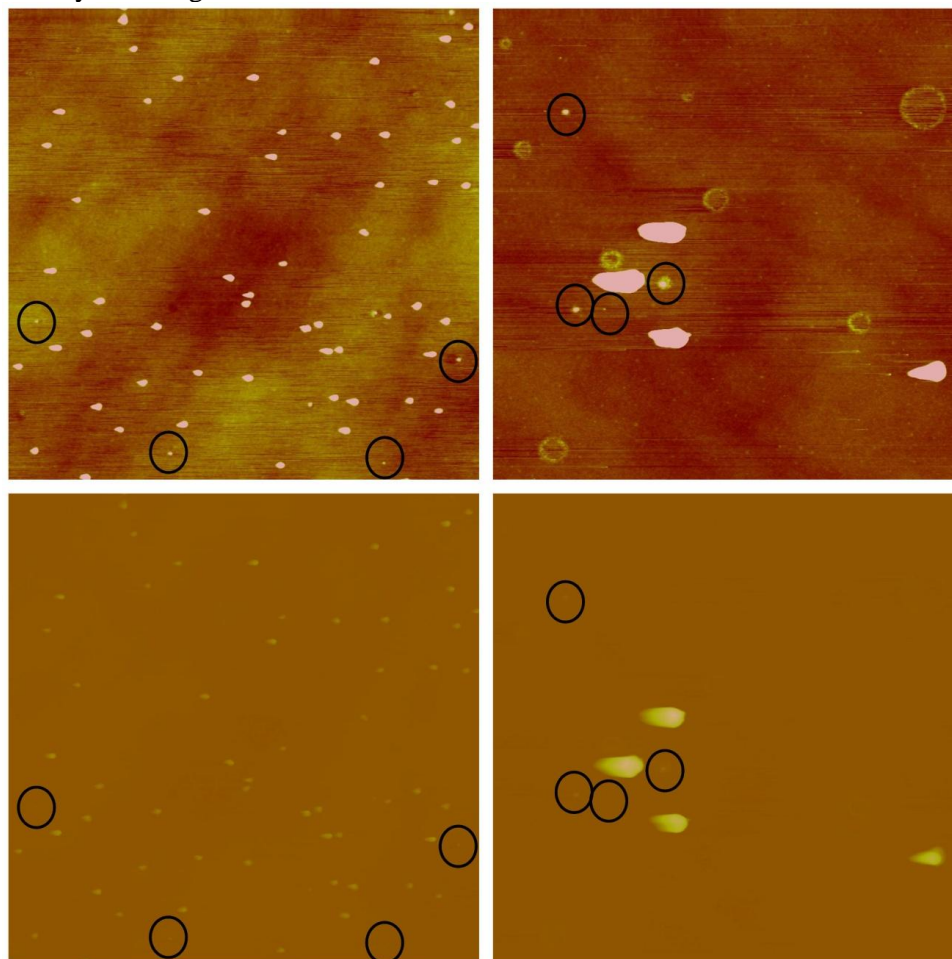


Figure SI-1. AFM images of (left column) sample D, nominally 20 nm citrate-capped AgNPs, and (right column) sample G, nominally 80 nm citrate-capped AgNPs. Images in top and bottom rows are from identical raw data file, top row, Z-scale = 10nm, bottom row, Z-scale = 350 nm. Edge of a single panel is 4.00 μm .

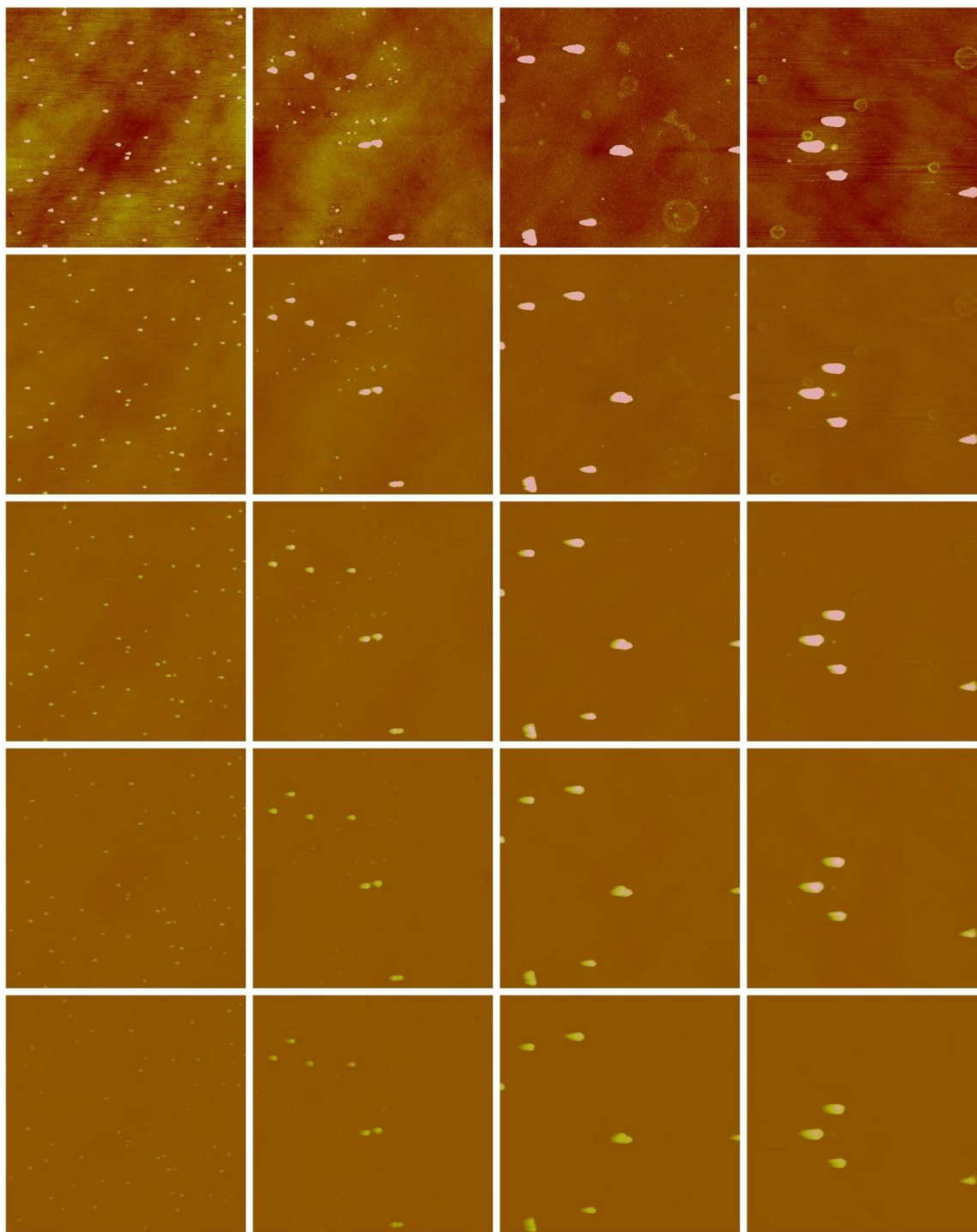


Figure SI-2. AFM images of AgNP samples D-G in columns from left to right. Z-scales of 10 nm, 50 nm, 125 nm, 225 nm, and 350 nm in rows from top to bottom. Edge of a single panel is 4.00 μm .

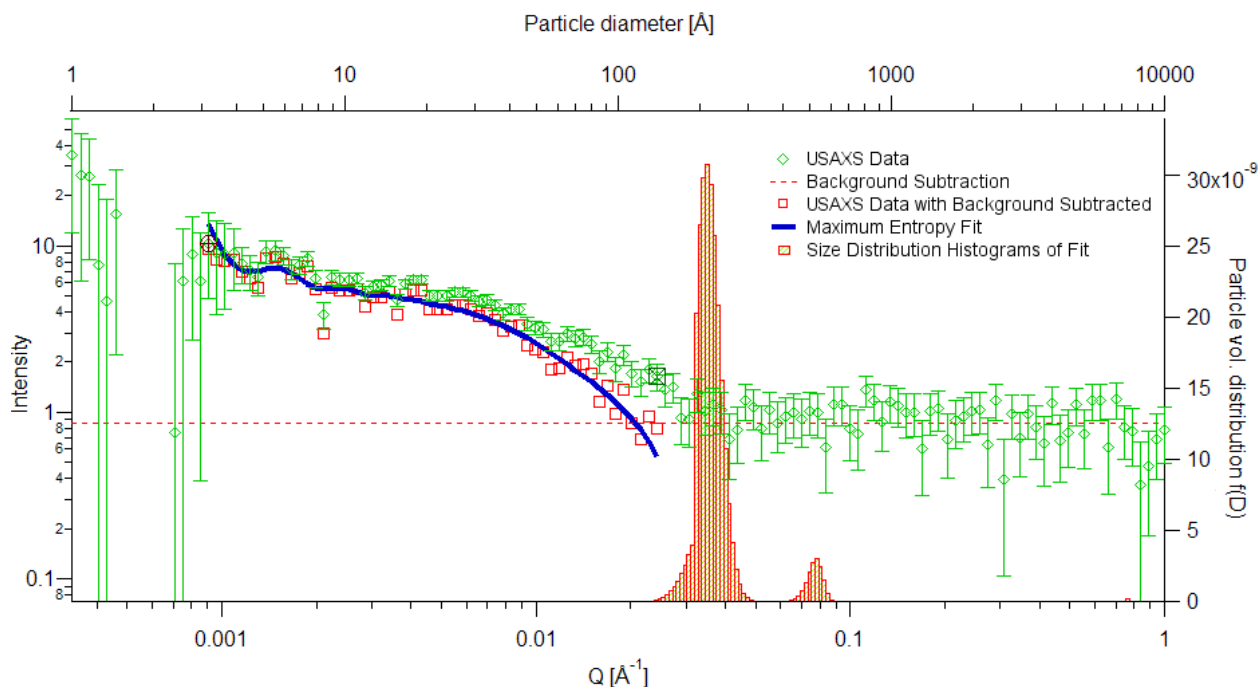


Figure SI-3. Illustrative analysis of very weak USAXS data for (nominally 20 nm silver particles) Sample f from Table 1. Background noise is accounted for by imposing a background subtraction (dashed red line) from all data points, and the background subtracted data (red squares) is put through an entropy maximization fit algorithm, resulting in a new scattering profile (blue line). The fit data are then analyzed in Irena and a size distribution is computed (red rectangles). In this case, judicious selection of the background value must be done in order to separate valuable from noisy data; this is why the given Q range was chosen ($0.0009 \text{ \AA}^{-1} < Q < 0.025 \text{ \AA}^{-1}$). Although particles $< 10 \text{ nm}$ and $> 100 \text{ nm}$, associated with high and low Q data, respectively, might be missed, non-existent particles won't be created by poor parameter estimation during the data analysis. (For less dilute suspensions, the flat background subtraction is less critical.)

Figure SI-3 shows size distribution results from the computational analysis of SAXS data using Irena 2, by Jan Ilavsky (references in main text). For such dilute concentrations of fine particles there is significant noise in the USAXS data at higher Q values ($Q > 0.03 \text{ \AA}^{-1}$), and consequently, the fit must be cut off prematurely. It is possible that smaller particles than shown may be present in the suspension. However, in these circumstances, the flat background must be carefully determined and subtracted from the scattering data before fitting with MaxEnt. Although the detectable size range is then restricted, we have greater quantitative certainty for the distribution within this size range. If one does not subtract a realistic background or recklessly extends the range of acceptable data in Q, artifacts can appear in the size distributions obtained. In this case, the above size distribution agrees well with other particle sizing techniques (shown in Figure 3 of the main text). This emphasizes the need for multiple orthogonal measurement techniques, as taking any one value as true can lead to unreliable results.

UV-vis absorbance spectra over time of AgNPs in EPA Moderately Hard Reconstituted Water, with Natural Organic Matter Fulvic Acid Standard I (MHRW-I).

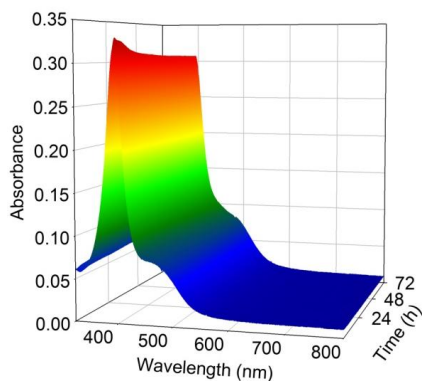


Figure SI-4. UV-vis absorbance spectra over time of “A” AgNPs (10 nm, citrate-capped) in MHRW-I.

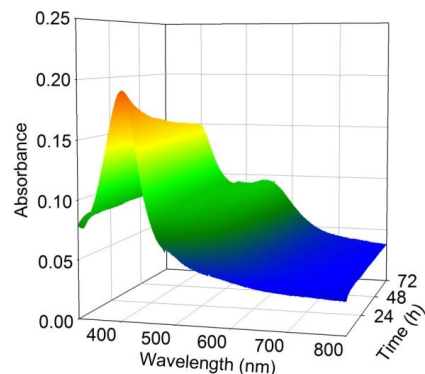


Figure SI-5. UV-vis absorbance spectra over time of “B” AgNPs (20 nm, citrate-capped) in MHRW-I.

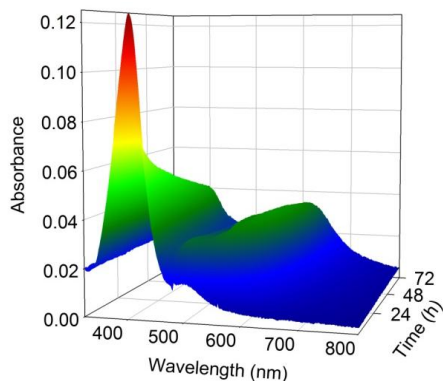


Figure SI-6. UV-vis absorbance spectra over time of “D” AgNPs (20 nm, citrate-capped) in MHRW-I.

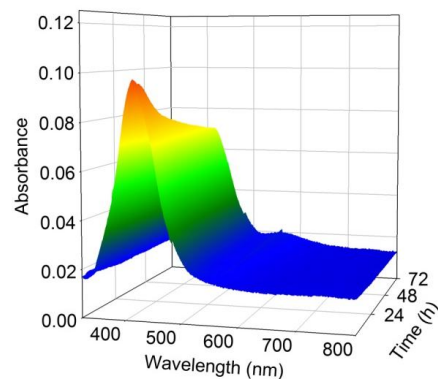


Figure SI-7. UV-vis absorbance spectra over time of “E” AgNPs (40 nm, citrate-capped) in MHRW-I.

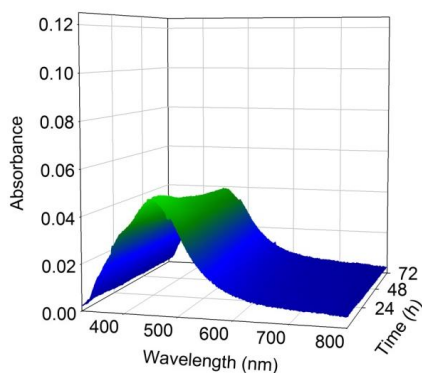


Figure SI-8. UV-vis absorbance spectra over time of “F” AgNPs (60 nm, citrate-capped) in MHRW-I.

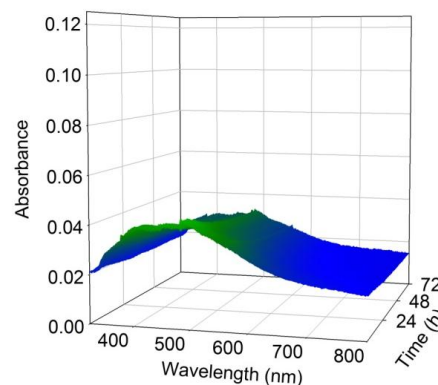


Figure SI-9. UV-vis absorbance spectra over time of “G” AgNPs (80 nm, citrate-capped) in MHRW-I.

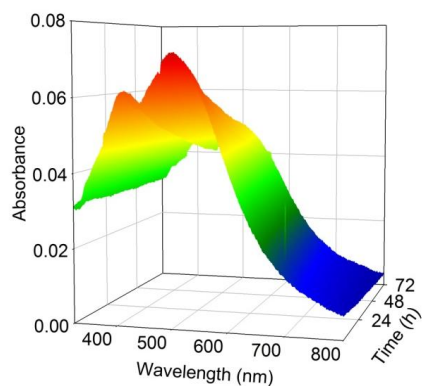


Figure SI-10. UV-vis absorbance spectra over time of “H” AgNPs (100 nm, citrate-capped) in MHRW-I.

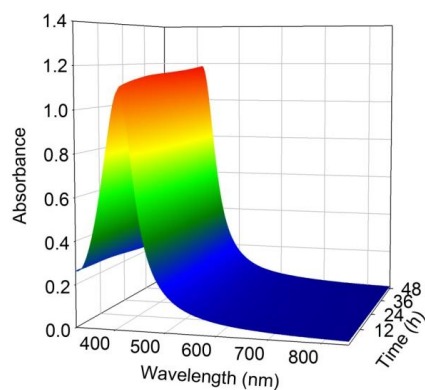


Figure SI-11. UV-vis absorbance spectra over time of “N” AgNPs (15 nm, starch-capped) in MHRW-I.

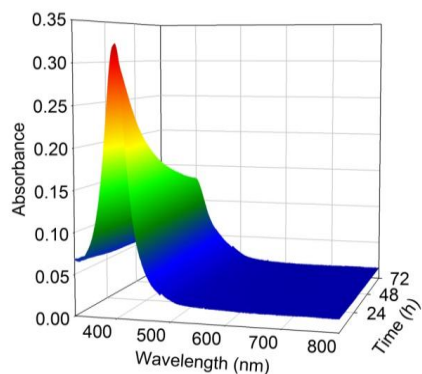


Figure SI-12. UV-vis absorbance spectra over time of “J” AgNPs (10 nm, PVP-capped) in MHRW-I.

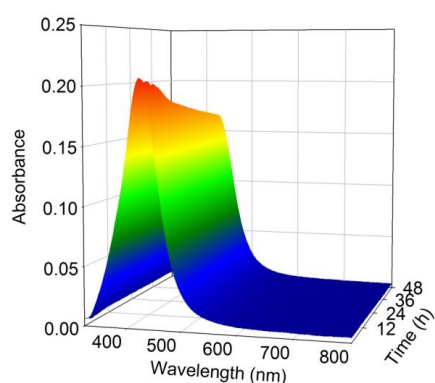


Figure SI-13. UV-vis absorbance spectra over time of “K” AgNPs (50 nm, PVP-capped) in MHRW-I.

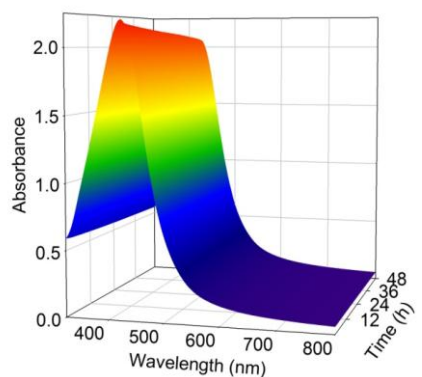


Figure SI-14. UV-vis absorbance spectra over time of “M” AgNPs (1 to 10 nm) in MHRW-I.

UV-vis absorbance spectra over time of AgNPs in EPA Moderately Hard Reconstituted Water + Natural Organic Matter Humic Acid Standard II (MHRW-II)

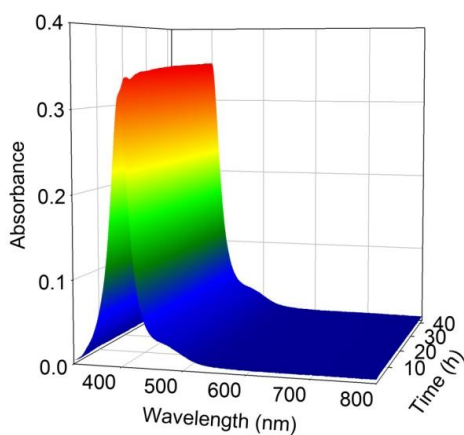


Figure SI-15. UV-vis absorbance spectra over time of “A” AgNPs (10 nm, citrate-capped) in MHRW-II.

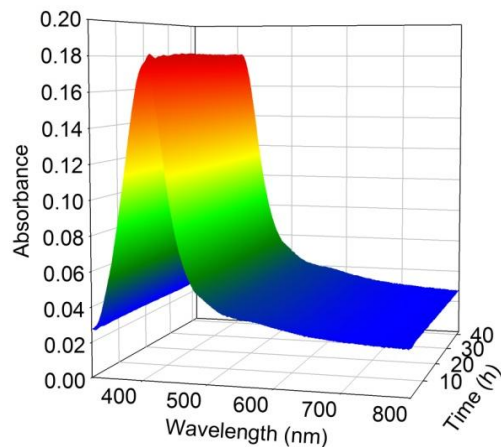


Figure SI-16. UV-vis absorbance spectra over time of “B” AgNPs (20 nm, citrate-capped) in MHRW-II.

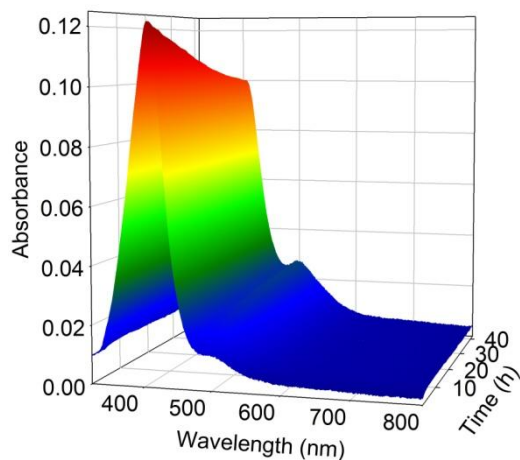


Figure SI-17. UV-vis absorbance spectra over time of “D” AgNPs (20 nm, citrate-capped) in MHRW-II.

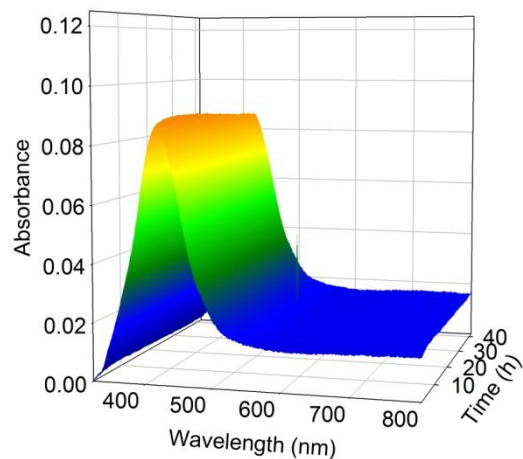


Figure SI-18. UV-vis absorbance spectra over time of “E” AgNPs (40 nm, citrate-capped) in MHRW-II.

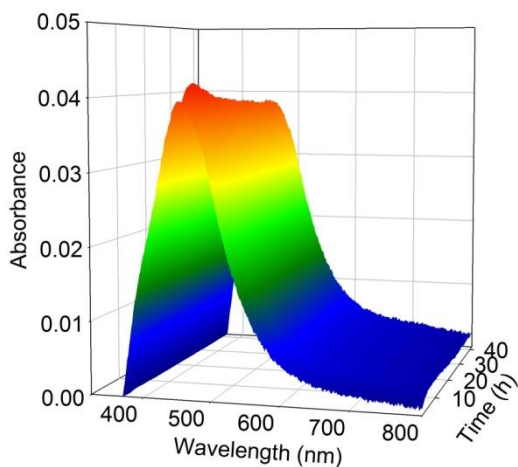


Figure SI-19. UV-vis absorbance spectra over time of “F” AgNPs (60 nm, citrate-capped) in MHRW-II.

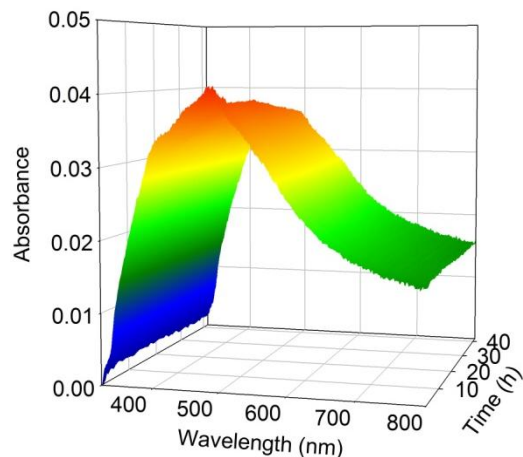


Figure SI-20. UV-vis absorbance spectra over time of “G” AgNPs (80 nm, citrate-capped) in MHRW-II.

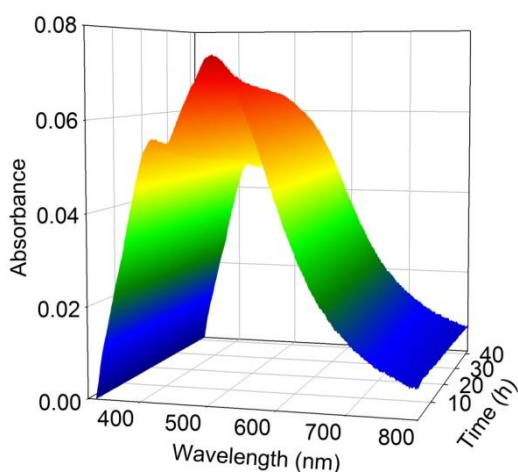


Figure SI-21. UV-vis absorbance spectra over time of “H” AgNPs (100 nm, citrate-capped) in MHRW-II.

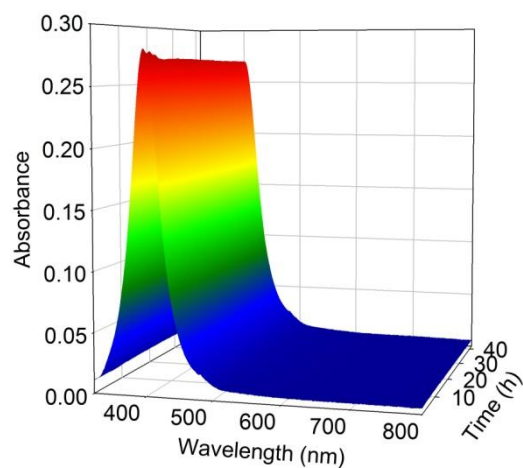


Figure SI-22. UV-vis absorbance spectra over time of “J” AgNPs (10 nm, PVP-capped) in MHRW-II.

UV-vis absorbance spectra over time of a powder PVP-capped AgNP material, dispersed in DI water by bath sonication and vortexing, serial dilutions of initial nominally $1 \text{ mg}\cdot\text{mL}^{-1}$ stock.

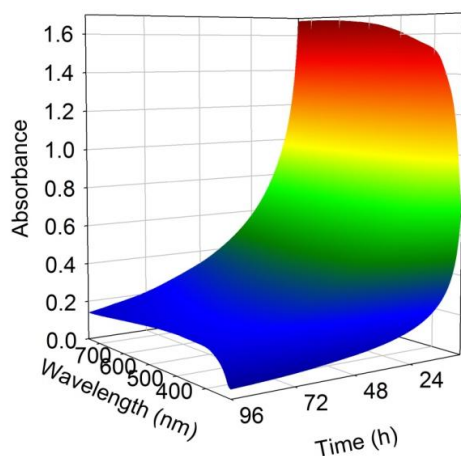


Figure SI-23. UV-vis absorbance spectra over time of “K” PVP-capped nominally 50 nm AgNPs in DI water, undiluted 1 mg mL^{-1} .

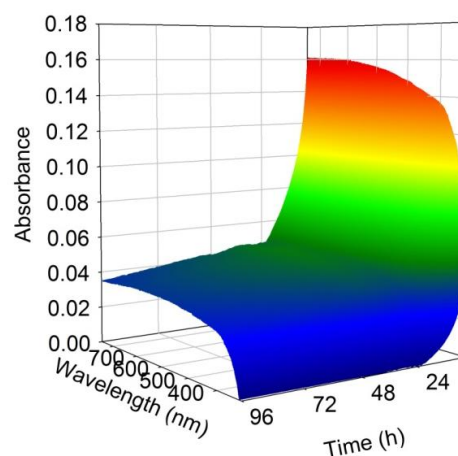


Figure SI-24. UV-vis absorbance spectra over time of “K” AgNPs in DI water, diluted 1 to 10.

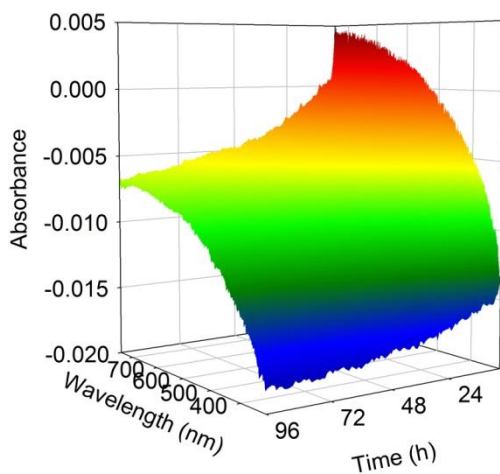


Figure SI-25. UV-vis absorbance spectra over time of “K” AgNPs in DI water, diluted 1 to 100.

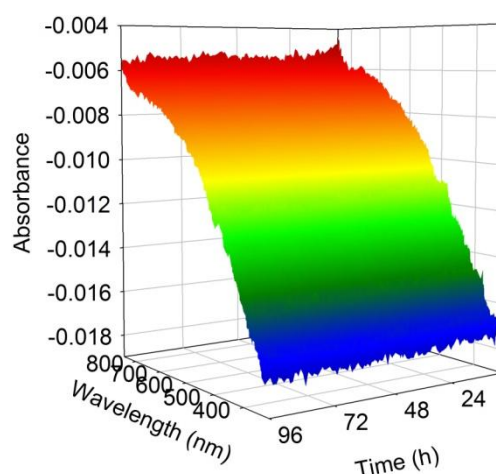


Figure SI-26. UV-vis absorbance spectra over time of “K” AgNPs in DI water, diluted 1 to 1000.

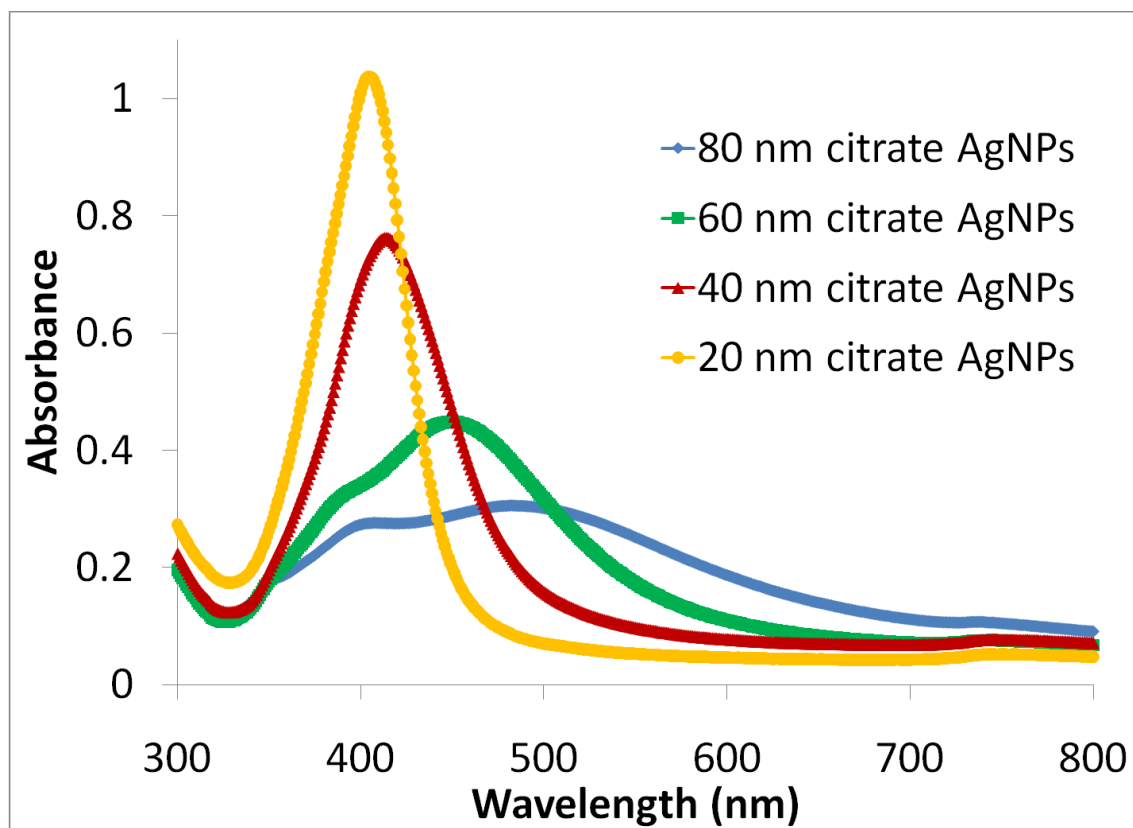


Figure SI-27. Absorbance spectra of four diameters of citrate-capped AgNPs in water, each with the same nominal mass of silver per mL of suspensions.